Integrated Coil Design for EV Wireless Charging Systems Using *LCC* Compensation Topology

Tianze Kan, *Student Member, IEEE*, Fei Lu, *Member, IEEE*, Trong-Duy Nguyen, Patrick P. Mercier, *Senior Member, IEEE*, and Chunting Chris Mi, *Fellow, IEEE*

***Abstract*—The double-sided *LCC* topology provides a highly efficient compensation method for electric vehicle (EV) wireless charging systems. However, the two compensated coils occupy a large volume. In order to address the volume increase as well as to be compatible with unipolar coil structures, which are widely applied in EV wireless charging systems, an integration method is introduced in this paper. Aspect ratios of the compensated coils are studied to minimize the respective coupling effect. With the proposed integration method, the extra coupling coefficients are either eliminated or decreased to a negligible level. A wireless charging system with the proposed integration method is built and the experimental results show that the system resonates at 85 kHz and delivers 3.09 kW with a dc–dc efficiency of 95.49% at an air gap of 150 mm. Furthermore, a comparison with the integration method into bipolar coil structures is presented and the results demonstrate that the system with the proposed integration method is more immune to front-to-rear and vertical misalignments.**

***Index Terms*—Electric vehicles (EVs), integrated coil design, *LCC* compensation topology, wireless power transfer.**

I. Introduction

An IMPORTANT application of wireless power transfer is to charge electric vehicles (EVs) [1]–[4]. Research areas in wireless charging for EVs include coil design [5]–[11], compensation topologies [12]–[17], power converters and corresponding control methods [18]–[21], foreign and living object detection [22]–[25], electromagnetic field radiations [26], [27], and environmental performance [28]. While all such areas are important, in this work we focus on optimizing coil structures, as they are the primary elements that set the theoretically achievable power transfer rate and efficiency. In general, it is desired to maximize their quality factor and geometrical arrangement: the higher quality factor and the coupling coefficient, the higher the system efficiency. In stationary wireless charging systems, there are mainly three coil structures [4]: 1) solenoid coil structures [5]; 2) unipolar coil structures [6]; and 3) bipolar coil structures (also referred to as DD coil structures) [7]. Since solenoid coils generate a double-sided magnetic flux pattern, half of which does not couple the receiver, they are not commonly adopted in EV charging applications. Instead, unipolar and bipolar coils are more popular. Unipolar coils, in which one pair of magnetic polarities is generated once the coils are excited, give a relatively higher coupling coefficient and generate vertical magnetic flux. Bipolar coils, in which two pairs of magnetic polarities are generated once the coils are excited, present a relatively lower coupling coefficient and develop horizontal magnetic flux. Experimental results in [8] show that bipolar coils have a better performance when horizontal misalignment occurs in the direction vertical to magnetic flux conduction path, which is the door-to-door direction.

To minimize the VA-rating of the power supply and maximize transferred power, coils in EV wireless charging systems are typically not driven directly, but instead, are compensated with a collection of capacitors and inductors [14]. Compensation in this manner can help achieve soft switching, thereby improving the efficiency of the corresponding power converters. It can also help deliver a constant current or constant voltage output, which may be advantageous in various applications [14], [15]. There are four basic compensation topologies where a single capacitor is used to resonate with the primary and secondary coils: series–series (SS), series–parallel, parallel–series, and parallel–parallel. Among them, SS is more widely used in EV wireless charging systems since the resulting resonance is independent of the coupling coefficient and load condition. However, it is not strictly necessary to employ only a single reactive compensation element per coil—for example, the double-sided *LCC* topology, proposed in [15], includes an inductor and two capacitors on each side of the circuit. The *LCC* topology inherits the advantages of the SS compensation topology while offering more flexibility to optimize the system efficiency and achieve zero voltage switching. However, compared to SS, the double-sided *LCC* topology has an obvious drawback: the two compensated inductors occupy a large volume.

In order to address the large volume increase, Li *et al*. [16] proposed integrating the compensated inductors into the main

Manuscript received November 27, 2017; accepted January 9, 2018. Date of publication January 17, 2018; date of current version August 7, 2018. This work was supported by the U.S. Department of Energy Graduate Automotive Technology Education Grant. Recommended for publication by Associate Editor Oscar Lucia. *(Corresponding author: Chunting Chris Mi.)*

T. Kan is with the Department of Electrical and Computer Engineering, San Diego State University, San Diego, CA 92182 USA, and also with the Department of Electrical and Computer Engineering, University of California San Diego, La Jolla, CA 92093 USA (e-mail: tikan@eng.ucsd.edu).

F. Lu and C. C. Mi are with the Department of Electrical and Computer Engineering, San Diego State University, San Diego, CA 92182 USA (e-mail: fei.lu@sdsu.edu; mi@ieee.org).

T.-D. Nguyen is with DENSO International America, Inc., Southfield, MI 48033 USA (e-mail: ntrduy@gmail.com).

P. P. Mercier is with the Department of Electrical and Computer Engineering, University of California San Diego, La Jolla, CA 92093 USA (e-mail: pmercier@ucsd.edu).

Color versions of one or more of the figures in this paper are available online at http://ieeexplore.ieee.org.

Digital Object Identifier 10.1109/TPEL.2018.2794448

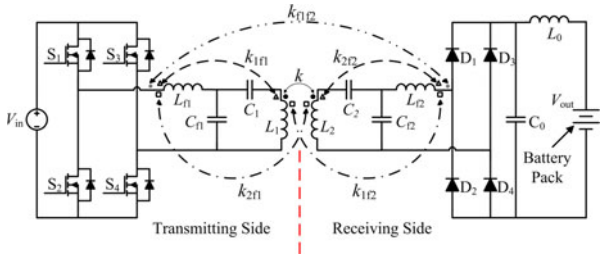

Fig. 1. Double-sided *LCC* compensation topology with integrated compensated coils and the cross couplings among the coils [17].

system coils. The integration method can effectively make an *LCC* wireless charging system more compact; however, three additional types of coupling coefficients manifest, as illustrated in Fig. 1: same-side coupling coefficients k_{1f1} and k_{2f2}, cross-side coupling coefficients k_{1f2} and k_{2f1}, and extra cross-side coupling coefficient k_{f1f2}. Li *et al*. analyzed the extra coupling coefficients and built a wireless charging system to transfer 6.0 kW with a dc–dc efficiency of 95.3%. Kan *et al*. [17] put forward a new integration method in which the extra coupling coefficients were either eliminated or minimized to a negligible level. While the presented analysis was simplified, the experimental results demonstrated a system that was able to deliver 3.0 kW with a dc–dc efficiency of 95.50%, which was competitive to that in [16]. However, the proposed integration method could be only utilized with bipolar coil structures.

This paper extends the work of [17] by analyzing and demonstrating an *LCC* compensation topology that is compact and efficient, and importantly, compatible with unipolar coil structures. Here, the coil structures are studied through ANSYS MAXWELL, in which the aspect ratio of the compensated coil is used as an important design specification to minimize the extra cross-side coupling coefficient. A wireless charging system with the proposed integration method is built to transfer 3.09 kW power with a dc–dc efficiency of 95.49%. Furthermore, the experimental results in [17] and this paper are compared, and the results show that the wireless charging system with the proposed integration method has a competitive performance under fully aligned condition and under door-to-door misalignment while achieving superior performance under front-to-rear and vertical misalignment. The contributions of this paper are concluded as:

1) it proposes an integration method compatible with unipolar coil structures in a wireless charging system using *LCC* compensation topology;
2) the proposed integration method eliminates the extra cross-side coupling coefficient, which is an advantage over the integration method in [17]; and
3) the wireless charging system with the proposed integration method has competitive performance under fully aligned condition and door–door misalignment, and superior performance over the system in [17] on front-to-rear and vertical misalignments.

II. Analysis

Integration makes the wireless charging system using *LCC* compensation topology more compact and the design of the

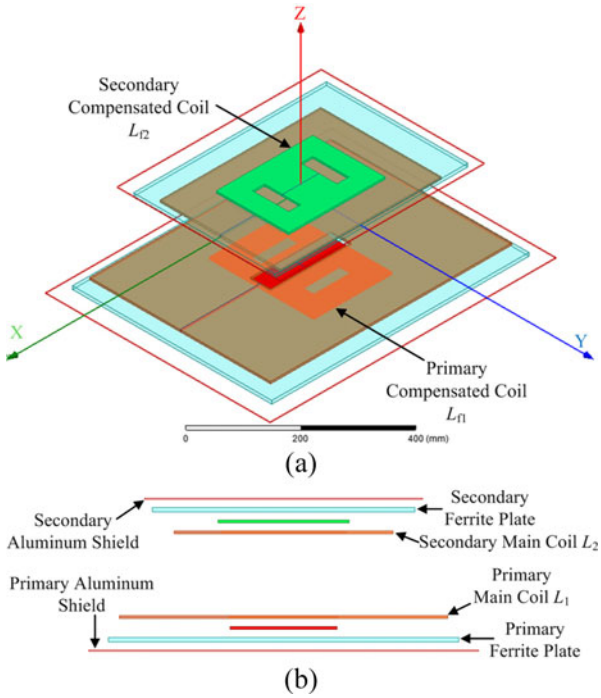

Fig. 2. (a) Overview and (b) cross-sectional view of coil structures with the proposed integration method.

system simpler. Fig. 2 shows the overview and cross-sectional side view of a coil structure with integrated compensated coils. On each side of the coil structures, there are four orderly arranged layers: the main coil, the compensated coil, a ferrite plate, and an aluminum shield. In particular, the main coils are unipolar and the compensated coils are bipolar. The power is transferred wirelessly from the primary side to the secondary side via the magnetic field generated by the two main coils. The ferrite plates and the aluminum shields provide sufficient magnetic shielding so that the generated magnetic field is concentrated within the coil structures. The compensated coils are not designed to transfer power, but tune the magnitudes of currents in the main coils so that a high efficiency will be achieved. Thus, the two compensated coils are preferred to have the lowest coupling effect between themselves and minimal interference with the two main coils.

In the newly proposed method, a bipolar compensated coil is integrated into a unipolar main coil, which is shown in Fig. 2. We take primary coils as an example. The net magnetic flux Ψ_{f11}, which is generated by the primary compensated coil L_{f1} and passing through the main coil L_1, can be expressed as

$$\Psi_{f11} = \iint \vec{B}_{f1} \cdot \vec{dS}_1 \tag{1}$$

where B_{f1} is the magnetic flux density and dS_1 is the surface element at the primary main coil. The magnetic flux, generated by a bipolar coil, flows from one of its magnetic dipoles to the other. The net magnetic flux is zero since the amount of magnetic flux enters into L_1 equals to the amount of magnetic flux flows out of it. Therefore, the coupling effect between L_1 and L_{f1} is eliminated and the coupling coefficient k_{1f1} is zero. Similarly,

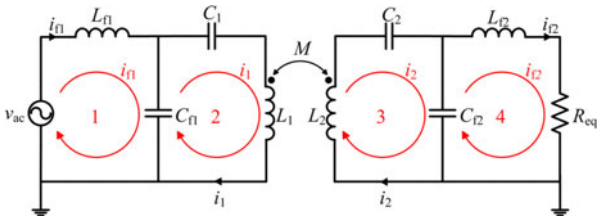

Fig. 3. Circuit with a double-sided compensation topology.

the net magnetic flux Ψ_{f12} generated by L_{f1} and passing through L_2 is zero and the coupling coefficient k_{2f1} between L_2 and L_{f1} is zero. The integration eliminates the same-side coupling coefficients and the cross-side coupling effects when fully aligned. Since the relative positions of the same-side coils do not change when misalignment occurs, the same-side coupling coefficients are still zero on both sides during misalignment. The relative positions of every two cross-side coils change and the cross-side coupling coefficients appear. Fortunately, the gap between every two cross-side coils is considerably large. The respective coupling coefficients are small and can be neglected at the frequency of interest, which will be verified by the experimental results in Section IV. The extra cross-side coupling coefficient exists all the time and it can be minimized to a negligible level, which will be studied and verified in the later sections. Therefore, only the main coupling coefficient is considered in the analysis. In addition, to simplify the analysis in this section, the equivalent series resistances (ESRs) of all the inductors and capacitors are neglected.

Fig. 3 shows the equivalent circuit of the double-sided *LCC* compensation topology. The full-bridge inverter and rectifier are omitted for simplicity. Instead, $v_{\rm ac}$ is the ac voltage after the inverter, $R_{\rm eq}$ is the equivalent resistance of the DC Load before the rectifier, and M is the mutual inductance between L_1 and L_2. In the circuit, L_{f1} resonates with C_{f1} and L_2 is combined with C_2 to resonate with C_{f2}; symmetrically, L_{f2} resonates with C_{f2} and the combination of L_1 and C_1 resonates with C_{f1}. Therefore, equations can be derived as

$$\begin{cases} \omega L_{f1} - \dfrac{1}{\omega C_{f1}} = 0, \omega L_2 - \dfrac{1}{\omega C_2} - \dfrac{1}{\omega C_{f2}} = 0 \\ \omega L_{f2} - \dfrac{1}{\omega C_{f2}} = 0, \omega L_1 - \dfrac{1}{\omega C_1} - \dfrac{1}{\omega C_{f1}} = 0 \end{cases} \tag{2}$$

where ω is the resonant angular frequency in radians. A mesh current method can be applied and the circuit is divided into four meshes, which is shown in Fig. 3. Solving the circuit equations, the input power equation can be derived as

$$P_{\rm in} = {\rm Re}\left(v_{\rm ac} \cdot i_{f1}^*\right) = \frac{M^2 R_{\rm eq} v_{\rm ac}^2}{\omega^2 L_{f1}^2 L_{f2}^2}. \tag{3}$$

In addition

$$\begin{cases} v_{\rm ac} = \dfrac{2\sqrt{2}}{\pi} V_{\rm in} \angle 0^\circ \\ M = k \cdot \sqrt{L_1 L_2} \\ R_{\rm eq} = \dfrac{8}{\pi^2} R_L = \dfrac{8 V_o^2}{\pi^2 P_o} \end{cases} \tag{4}$$

where $V_{\rm in}$ is the dc input voltage of the full bridge inverter, k is the main coupling coefficient between L_1 and L_2, R_L is the load resistance, V_o is the dc battery voltage, and P_o is the output power. In this section, the power loss is ignored and $P_{\rm in}$ equals to P_o. After combining (3) with (4), the power can be rewritten as

$$P_{\rm in} = P_o = \frac{8k\sqrt{L_1 L_2} V_{\rm in} V_o}{\pi^2 \omega L_{f1} L_{f2}}. \tag{5}$$

III. System Design

A wireless charging system from the dc input to dc battery mainly consists of three parts: an inverter, a rectifier, and coils with compensation networks. The power loss of the wireless charging system originates from the three parts. The SiC MOSFETs are selected for the inverter, while the diodes are chosen for the rectifier. Since zero voltage switching is achieved in the inverter stage, most of the power loss in the inverter and rectifier is the conduction loss of the MOSFETs and diodes, which is approximately 31 W in a 3.0 kW wireless charging system. This contributes to 1% efficiency drop. Therefore, the majority of the system power loss is from the coils and compensation networks. In a wireless charging system with a double-sided *LCC* compensation topology, there are eight circuit components: four inductors (i.e., coils) and four capacitors. The power loss in the circuit components is determined by their ESRs. The ESR of an inductor is determined by its quality factor, frequency, and inductance value, while the ESR of a capacitor depends on its dissipation factor, frequency, and capacitance. Under the resonant condition, the frequency is fixed and based on (2), the capacitor values are determined by the inductor values. Therefore, the design is focused on optimizing the values of the four inductors so that the system is able to achieve the highest efficiency at the desired output power. Since the power transfer replies on the coupling between the two main coils, the maximum coupling coefficient is desired within the main coil dimensions. The dimensions of the primary and secondary main coils are "600 mm $\times$ 450 mm $\times$ 4 mm" and "400 mm $\times$ 300 mm $\times$ 4 mm." The secondary is relatively smaller since it is installed on the vehicle. Here, the dimensions of the main coils remain the same with those in [17] for a fair comparison in Section V. The air gap between the two main coils is 150 mm. The coupling coefficient is closely related to the coil geometry and varies with the primary and secondary coil widths in Fig. 4(a). It is maximized at 0.2305 when the primary coil width is 200 mm and secondary coil width is 90 mm, which is shown in Fig. 4(b).

The two main coils are wound by the same type of litz wires. The required coil widths are achieved and the turn numbers are different. The self-inductances of the main coils are determined. Based on [17], the efficiency of a wireless charging system using the double-sided *LCC* compensation topology is mainly determined by the ESRs of the inductors and the capacitors. In order to achieve the highest efficiency at the desired output power, the same design procedures as in [17] are followed and Fig. 5 presents the calculated results from MathCAD. Based on (4), when the output power is 3.0 kW and the battery voltage is 340 V, the equivalent load resistance is 31.23 Ω. The efficiency

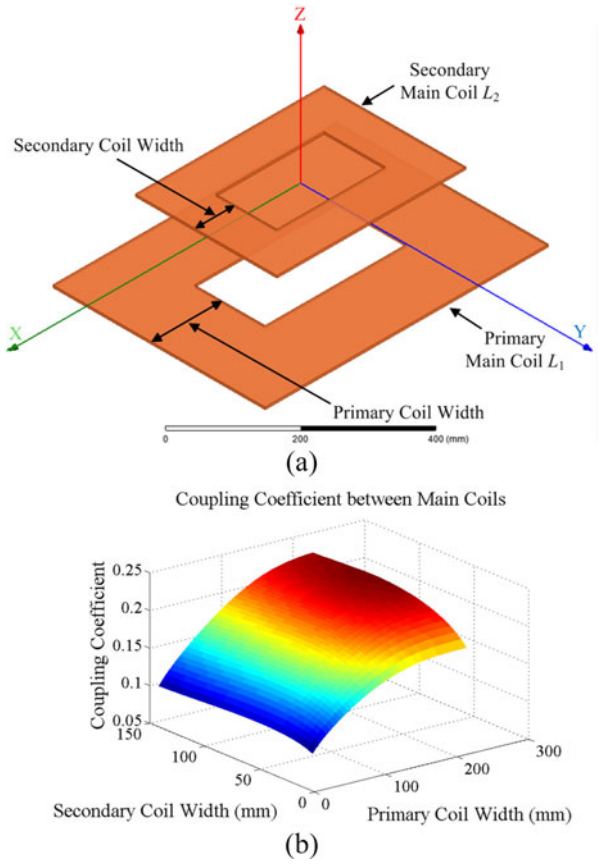

Fig. 4. (a) Design variables in the main coil simulation model and (b) simulation results on the main coupling coefficient.

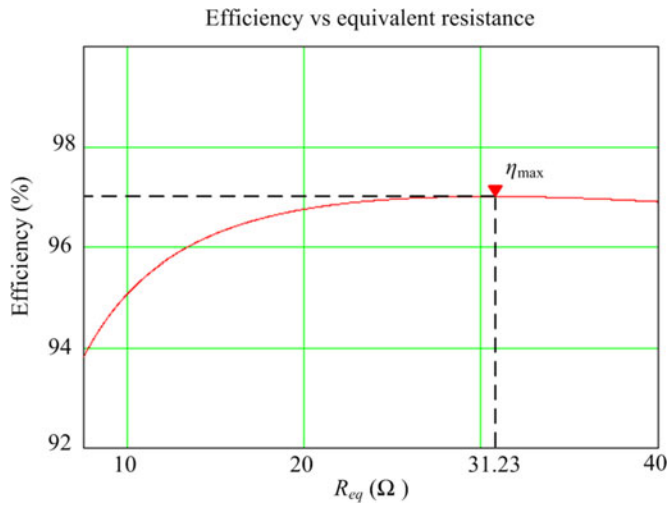

Fig. 5. Efficiency curve.

is maximized at 97.0% in Fig. 5. Here, the power loss from the inverter and rectifier is ignored when calculating the efficiency. The required self-inductances of the primary and secondary compensated coils are 56 and 43 μH, respectively.

With the required values, the compensated coils are designed by employing ANSYS MAXWELL. Since the extra cross-side coupling between the two compensated coils is unexpected from the design point of view in this paper, the minimum extra

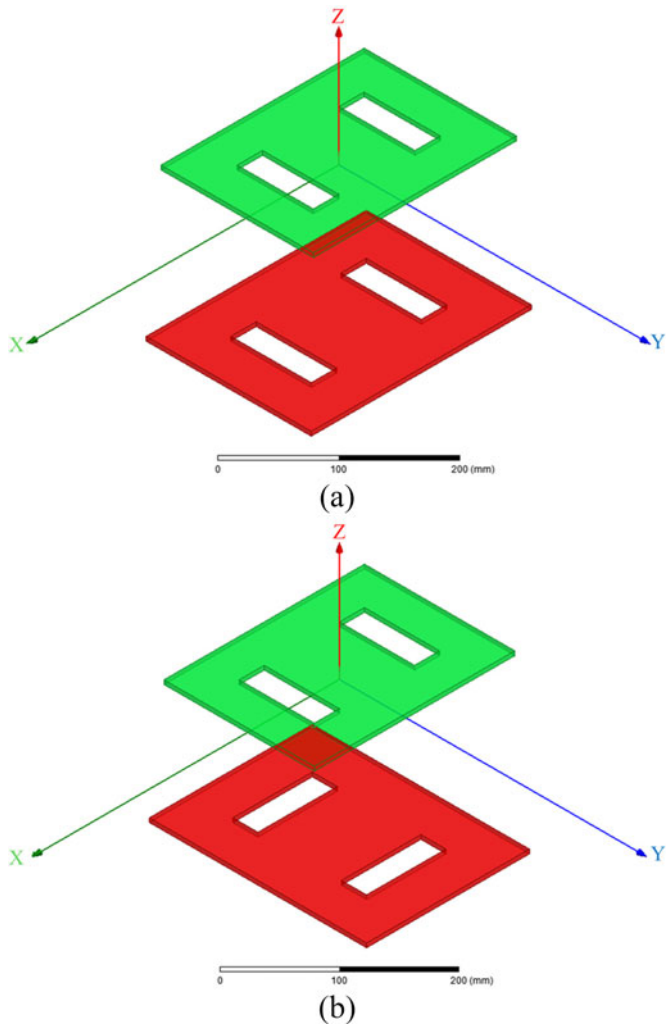

Fig. 6. Two placements: (a) placement I and (b) placement II.

cross-side coupling is the goal. As analyzed in Section II, the bipolar coils are selected as the compensated coils and integrated into the unipolar main coil structures. Different aspect ratios of the compensated coils are studied to obtain the minimum coupling. The aspect ratio is defined as "*W*/*L*," where *W* is the length of the compensated coil in the *Y*-direction and *L* is the length in the *X*-direction. The magnetic flux generated by a bipolar coil is single-directional rather than isotropic. Therefore, the placement of the two compensated coils affects the coupling coefficient between them. Two kinds of placement as shown in Fig. 6 are studied: 1) placement I, in which the two coils are fully aligned; and 2) placement II, in which the two coils are misaligned with an angle of 90°. In addition, the areas of the primary and secondary compensated coils are approximately fixed at 50 000 and 40 000 mm^2 in all simulation cases.

A. *Placement I*

For placement I, the studied aspect ratios are "1:2," "3:4," "1:1," and "4:3" for both the primary and secondary compensated coils. Simulation results are shown in Fig. 7(a) and the minimum coupling coefficient is 0.019 with the primary aspect

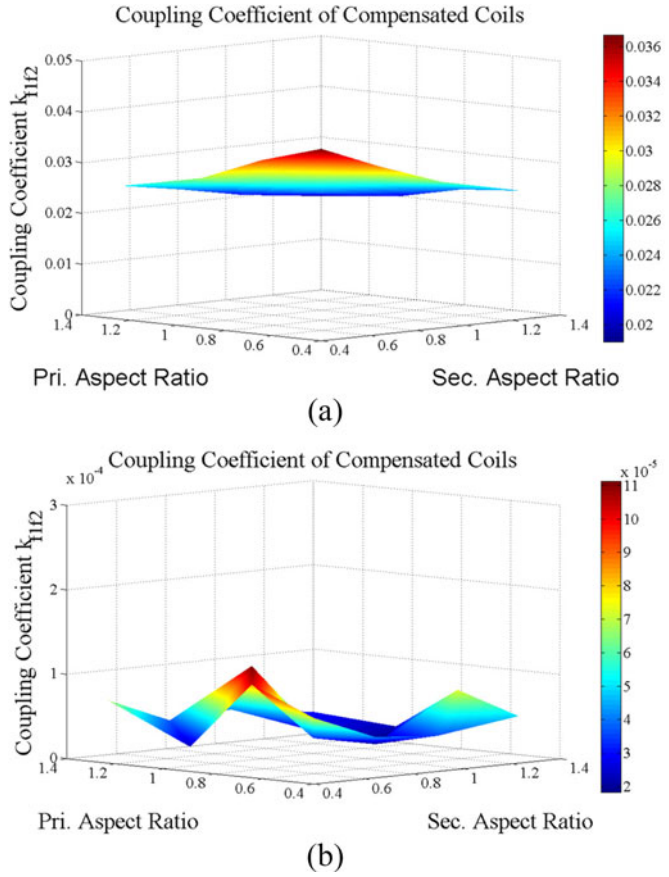

Fig. 7. Simulation results of k_{f1f2} at (a) placement I and (b) placement II.

ratio of "4:3" and the secondary aspect ratio of "3:4." Additionally, the inductances of the primary and secondary compensated coils are kept at 56 and 43 μH within 3% fluctuations in all simulation cases.

B. Placement II

Placement II is shown in Fig. 6(b) and the same aspect ratios are studied for both the primary and secondary compensated coils. As shown in Fig. 7(b), the extra cross-side coupling coefficients are close to zero. Also, the compensated inductances remain at the desired values with 3% fluctuations in all simulation cases. The primary aspect ratio of "3:4" and the secondary aspect ratio of "4:3" are selected for the primary and secondary compensated coils for the purpose of winding the coils easily.

In addition, in order to verify that the compensated coils are the most compact with the proposed integration method, simulation studies of compensated coils in ferrite-core and air-core types are conducted. Fig. 8 shows the simulation models and in particular, the ferrite-core is made up of two E-cores. The compensated coils in different types are simulated to achieve the desired inductance values and their volumes are compared in Table I. It is obvious that the air-core coils occupy the most space, the ferrite-core coils less, and the integrated coils the least. Furthermore, the integrated coils have two more advantages over the ferrite-core coils: 1) the integrated coils are planar, which

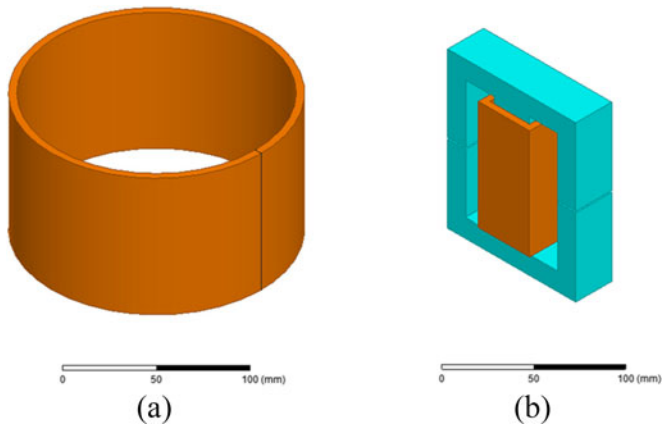

Fig. 8. Simulation models of (a) air-core coil and (b) ferrite-core coil.

TABLE I
VOLUME FOR EACH COIL

Coil type	L_{f1}	L_{f2}
Air core	1.810×10^6 mm^3	1.609×10^6 mm^3
Ferrite core	3.712×10^5 mm^3	3.740×10^5 mm^3
Integrated	2.250×10^5 mm^3	1.800×10^5 mm^3

is easier for packaging; and 2) the integrated coils are more cost beneficial from material's point of view. The integrated coil needs more litz wire, while ferrite-core coils require four E-cores. The price of lite-wire is $1.16 per meter, while one E-core costs $18.75. By calculation, the integrated coils save $50.99 per wireless charging system.

The compensated coils are wound and measured. The resonant frequency is constant at 85 kHz. Once the inductances are determined, the capacitors C_1, C_2, C_{f1}, and C_{f2} can be calculated based on (2). Specifically, as stated in [16], the capacitor C_2 is 8% larger than the calculated value to guarantee zero voltage switching of the MOSFETs.

IV. EXPERIMENT

Experiments were conducted from dc power source to dc electronic load. A full-bridge inverter and a full-bridge rectifier are used for power conversion between ac and dc. Based on our experience, the current densities in coils are desired to be less than 2.5 A/mm^2. Therefore, coils are wound with 800-strand AWG-38 litz wires. Ferrite plates are made of 3C95 ferrite bars. On each side of the wireless charging system, the main coil, the compensated coil, and the ferrite plate are wound or placed in separate plexiglass boards, which provides sufficient insulation and guarantees safe and reliable operation. The measured circuit parameters are compared with the respective simulation results in Table II. The measured values match well with the simulated values. Based on series-aiding and series-opposing method introduced by [29], different coupling coefficients under the fully aligned condition and four misaligned conditions are measured. Here, under each of the four misaligned conditions, misalignment only occurs in a single direction. For example, when the

TABLE II
CIRCUIT PARAMETERS

Parameters	Simulated values	Measured values	Error
Primary main coil inductance L_1	229.47 μH	242.10 μH	5.21%
Primary compensated coil inductance L_{f1}	56.30 μH	60.08 μH	6.29%
Secondary main coil inductance L_2	182.30 μH	191.21 μH	4.66%
Secondary compensated coil inductance L_{f2}	43.61 μH	43.57 μH	0.09%
Primary capacitor C_1	19.70 nF	19.26 nF	2.28%
Primary compensated capacitor C_{f1}	58.38 nF	58.35 nF	0.05%
Secondary capacitor C_2	25.80 nF	25.68 nF	0.47%
Secondary compensated capacitor C_{f2}	79.67 nF	80.47 nF	1.37%

TABLE III
MEASURED INDUCTANCE VALUES

Conditions	L_1	L_2	L_{f1}	L_{f2}
Fully aligned	242.10 μH	191.21 μH	60.08 μH	43.57 μH
$Z_{misalign} = 50$ mm	242.24 μH	188.82 μH	59.93 μH	43.52 μH
$X_{misalign} = 100$ mm	244.77 μH	190.61 μH	59.99 μH	43.54 μH
$Y_{misalign} = 100$ mm	245.81 μH	191.44 μH	60.06 μH	43.50 μH
$Y_{misalign} = 150$ mm	247.41 μH	191.52 μH	59.84 μH	43.45 μH

TABLE IV
MEASURED COUPLING COEFFICIENTS

Conditions	k	k_{1f1}	k_{2f2}	k_{1f2}	k_{2f1}	k_{f1f2}
Fully aligned	0.2208	0.0028	0.0015	0.0002	0.0029	0.0006
$Z_{misalign} = 50$ mm	0.1439	0.0026	0.0062	0.0001	0.0011	0.0007
$X_{misalign} = 100$ mm	0.1886	0.0026	0.0057	0.0205	0.0055	0.0002
$Y_{misalign} = 100$ mm	0.1426	0.0008	0.0060	0.0010	0.0490	0.0011
$Y_{misalign} = 150$ mm	0.0869	0.0021	0.0058	0.0014	0.0474	0.0009

misalignment in the *Z*-direction is 50 mm, the misalignment in the *X*- and *Y*-direction is zero. The results on measured inductances and coupling coefficients are listed in Tables III and IV. It is demonstrated by the measured results that the inductance values remain almost the same, only the main coupling coefficient should be considered, and other five coupling coefficients are negligible at the frequency of interest.

The design parameters are presented in Table V. The input dc voltage and dc load voltage are both 340 V. The resonant frequency is at 85 kHz and the air gap is 150 mm, which is appropriate for passenger cars. The output power is designed to be 3.0 kW. The experiment setup of the coil structures is shown in Fig. 9. The bipolar compensated coils are integrated into the unipolar main coils. Moreover, in each turn of primary main coils, there are two litz wires in parallel. This not only ensures the coil width is the same as that in the simulation of Section III but also guarantees the primary main self-inductance is within the reasonable range.

The experiment is conducted when the primary and secondary coil structures are fully aligned and the respective waveforms

TABLE V
SYSTEM SPECIFICATIONS

Parameters	Designed values
Input dc voltage	340 V
Output dc voltage	340 V
Primary main coil dimension	600 mm × 450 mm × 4 mm
Primary ferrite plate dimension	640 mm × 496 mm × 8 mm
Primary shield dimension	711 mm × 559 mm × 2 mm
Secondary main coil dimension	400 mm × 300 mm × 4 mm
Secondary ferrite plate dimension	480 mm × 352 mm × 8 mm
Secondary shield dimension	508 mm × 406 mm × 2 mm
Air gap	150 mm
Resonant frequency	85 kHz
Maximum output power	3.0 kW

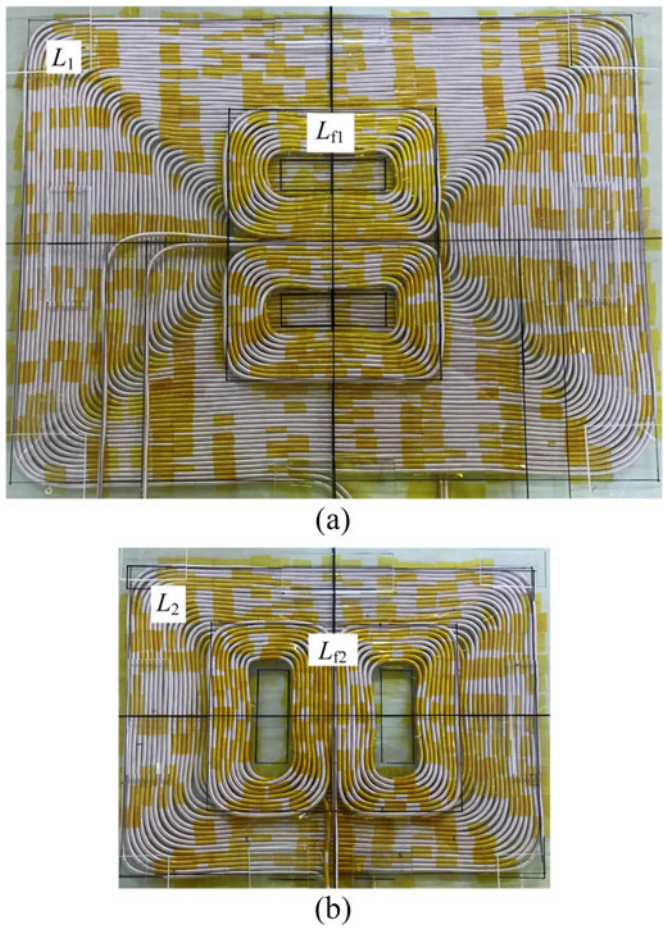

Fig. 9. Experiment setup of (a) primary coils and (b) secondary coils.

are shown in Fig. 10. The input and output dc voltages are both 340 V. The input ac current i_{f1} is almost in phase with the input ac voltage v_{ac} and a small phase shift is to guarantee the soft switching of the MOSFETs $S_1 - S_4$. As can be seen from Fig. 10, when S_1 and S_4 are turned OFF, the instantaneous value of i_{f1} is approximately 4.0 A, which is larger than zero. Therefore, the drain-to-source voltages of S_1 and S_4 are zero when they are turned OFF. In addition, based on [17], a current value of 4.0 A is sufficient to charge the parasitic capacitors of S_2 and S_3 during the dead time so that the drain-to-source voltages of both S_2 and

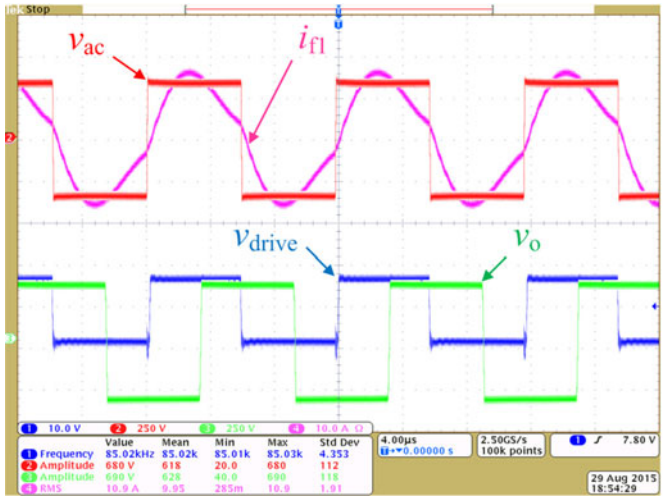

Fig. 10. Waveforms when coil structures are fully aligned at maximum power.

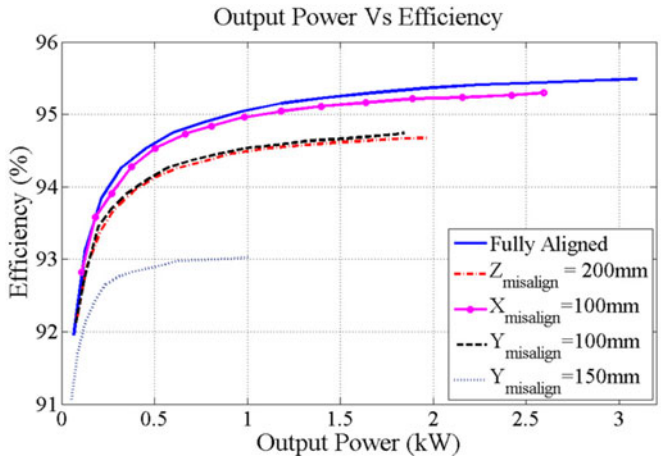

Fig. 11. Experimental results on output power versus efficiency.

S_3 are almost zero when they are turned ON. Thus, zero voltage switching is realized.

Experiment on misalignment in different directions is also conducted and all the experimental results are presented in Fig. 11. When the system is fully aligned, the wireless charging system delivers 3.09 kW power with a dc–dc efficiency of 95.49% at an air gap of 150 mm. When misalignment occurs, the main coupling coefficient k decreases, while other parameters remain almost the same and there is almost no other extra coupling coefficient. The output power P_o drops with k when the same dc input voltage and load voltage are applied. Fig. 12 shows the normalized values for P_o and k. The rated values for P_o and k are 3.09 kW and 0.2208 when the system is fully aligned. In Fig. 12(a) and (b), P_o drops at the same rate with k when misalignment occurs in the *Z*- or *X*-direction. The differences are within 2%, which validates (5) in Section II. In Fig. 12(c), when misalignment occurs in the *Y*-direction, the maximum difference is approximately 10%. It is because the cross-side coupling coefficient k_{2f1} arises as the misalignment increases. However, k_{2f1} is under 0.05 under all conditions of misalignments in the *Y*-direction, which is shown in Table IV.

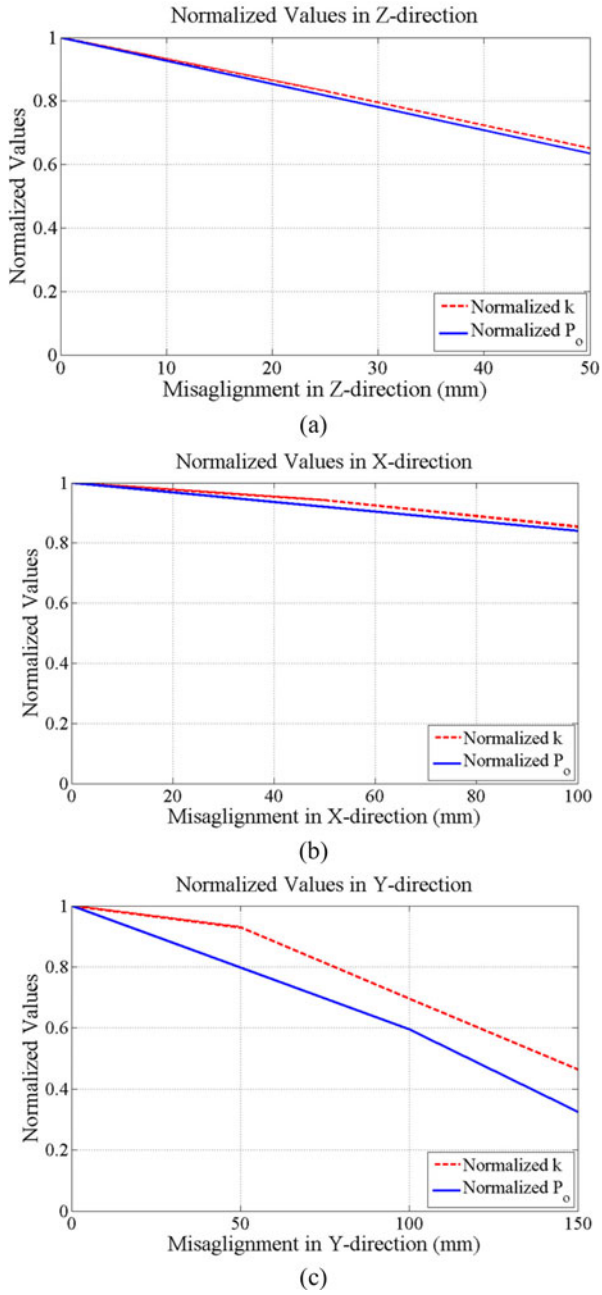

Fig. 12. Normalized values in (a) *Z*-direction, (b) *X*-direction, and (c) *Y*-direction.

Therefore, the difference is acceptable and the adverse effect can be ignored. Hence, with the integration method, the extra coupling coefficients are eliminated or minimized to a negligible level and the wireless charging system is more compact. Furthermore, the efficiency of the wireless charging system is kept high. Thus, the experiment verifies the proposed idea.

V. Discussion

Two integration methods, named as integration into bipolar coils method (IB method) and integration into unipolar coils (IU method), are separately given in [17] and this paper for wireless charging systems using the *LCC* compensation topology. In this

TABLE VI
PHYSICAL DESIGN COMPARISON

Quantity	Items	IB method	IU method
Total length	Litz wires	92.92 m	86.58 m
Voltage/Current-rating (rms)	C_1	1205 V/12.69 A	923 V/9.45 A
	C_{f1}	374 V/16.60 A	439 V/13.67 A
	C_2	803 V/13.97 A	997 V/14.25 A
	C_{f2}	405 V/20.76 A	442 V/19.70 A

section, the physical design parameters and system performance are compared between the two wireless charging systems with the two integration methods. Moreover, in order to make a fair comparison, power converters and the dimensions of the main coils, the ferrite plates, and the aluminum shield are all the same. An interoperability study of the proposed integrated coil structure with bipolar and unipolar coil structures is conducted at the end of this section.

A. Physical Design Parameters

From material's point of view, the two wireless charging systems with the two integration methods employ the same power converters and are controlled by the same microcontroller. Furthermore, the ferrite plates and aluminum shields are the same in the two systems. The difference occurs in the total length of litz wires used in the two systems and the voltage and current ratings of the capacitors at 3.0 kW output power. Table VI presents the comparison results. The total lengths of the litz wires used in two systems are almost the same and the voltage and current ratings are similar for respective capacitors.

B. System Performance

Power and efficiency are the two main indexes in the system performance of a wireless charging system. As indicated by the experimental results on horizontal misalignment (i.e., *X*-direction and *Y*-direction) in [17] and this paper, the output power of each system is different in the *X*-direction from that in the *Y*-direction even though the same input dc voltage is applied and both misalignments are 100 mm. Moreover, once an EV is parked, it is more difficult for a driver to adjust the EV in the door-to-door direction than in the front-to-rear direction. Therefore, in each system, the direction with a higher output power is aligned with EV's door-to-door direction and the direction with a lower output power is aligned with EV's front-to-rear direction.

Fig. 13 shows the comparison of the system performance of the systems when the system is fully aligned, door-to-door misalignment is 100 mm, front-to-rear misalignment is 100 mm, and vertical misalignment is 50 mm. Efficiencies are compared when the same amount of output power is delivered by the two systems. The two systems have almost the same efficiency when the output power is the same when the system is fully aligned and door-to-door misalignment is 100 mm. However, the system with the IU method has a relatively higher efficiency when front-to-rear misalignment is 100 mm and vertical misalignment is

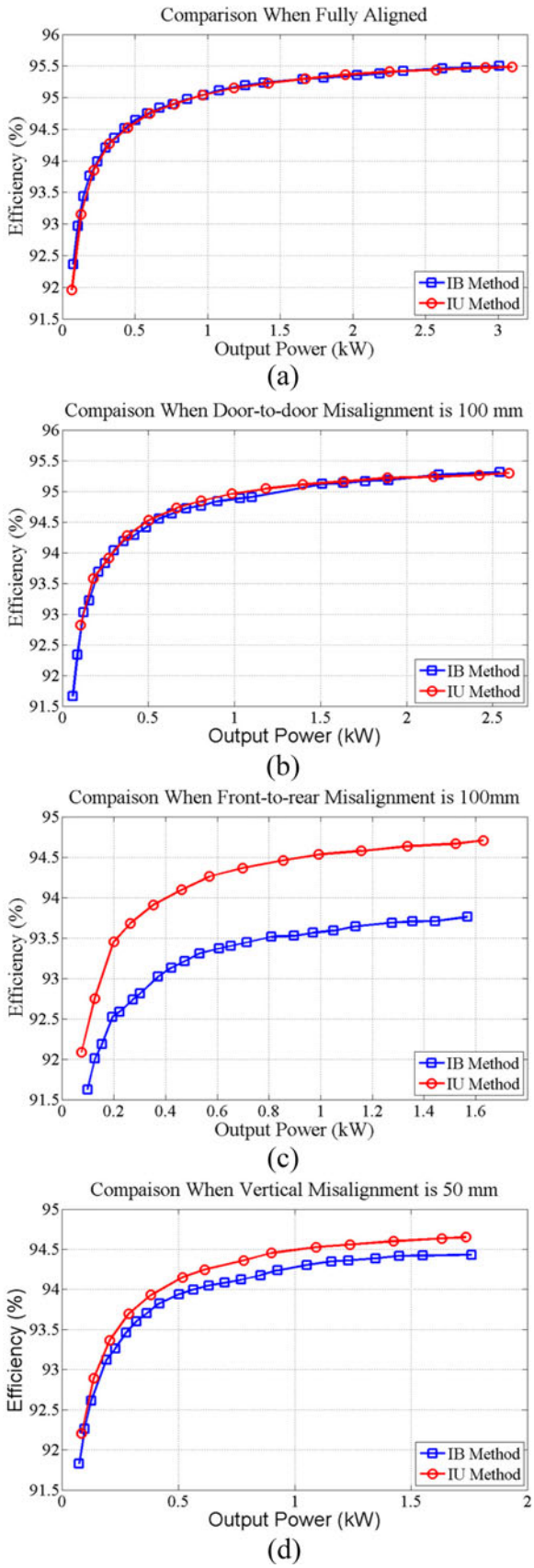

Fig. 13. Comparison on system performance when (a) system is fully aligned, (b) door-to-door misalignment is 100 mm, (c) front-to-rear misalignment is 100 mm, and (d) vertical misalignment is 50 mm.

TABLE VII
MAIN COUPLING COEFFICIENT IN DIFFERENT SCENARIOS

Scenarios	IB method		IU method	
	Value	Dropped (%)	Value	Dropped (%)
Fully aligned	0.1877	0	0.2208	0
Door-to-door misalignment = 100 mm	0.1578	15.9	0.1886	14.6
Front-to-rear misalignment = 100 mm	0.1042	44.5	0.1537	30.4
Vertical misalignment = 0 mm	0.1045	44.3	0.1439	34.8

50 mm. It is because the main coupling coefficient in the system with the IU method drops more slowly than that in the system with the IB method as front-to-rear misalignment or vertical misalignment occurs. As shown in Table VII, k separately drops 30.4% and 34.8% from its original value in the system with the IU method when front-to-rear misalignment is 100 mm and vertical misalignment is 50 mm, while 44.5% and 44.3% in the system with the IB method.

Thus, based on the comparison of the physical design parameters and system performance, both systems employ a similar amount of materials and perform well in power and efficiency. The wireless charging system with the IU method is comparatively better since it transfers power with a higher efficiency at the same output power level when front-to-rear or vertical misalignment occurs.

C. Interoperability Study

An interoperability study on the proposed coil structure with bipolar and unipolar coil structures has been conducted. The primary coil structure is either bipolar or unipolar, while the secondary coil structure employs the proposed integrated coil structure, in which a bipolar compensated coil is integrated into a unipolar main coil. The coupling coefficients under the fully aligned condition are analyzed and measured. In one case, the primary coil is bipolar, as shown in Fig. 14(a), the net amount of magnetic flux generated by L_1 and passing through L_2 is zero. Therefore, the main coupling coefficient is zero. The primary main coil L_1 and secondary compensated coil L_{f2} are both bipolar and fully aligned. The coupling coefficient k_{1f2} exists and a voltage will be induced from L_1 to L_{f2}. However, power still cannot be transferred. It is because the secondary main coil L_2, together with two capacitors C_2 and C_{f2}, forms a parallel resonant circuit, of which the impedance is infinite under the resonant condition. In the other case, the primary coil is unipolar, as shown in Fig. 14(b), which is the same as the one in this paper. The coupling coefficients k is maximized and k_{1f2} is almost zero. The power transfer capability of the two main coils is maximized. Both the simulation and experimental results are summarized in Table VIII. In order to successfully transfer power, the two main coils in a wireless charging system must be in the same type and fully aligned. Furthermore, for wireless charging systems using *LCC* compensation topology, the integration method should be selected based on the main coil type.

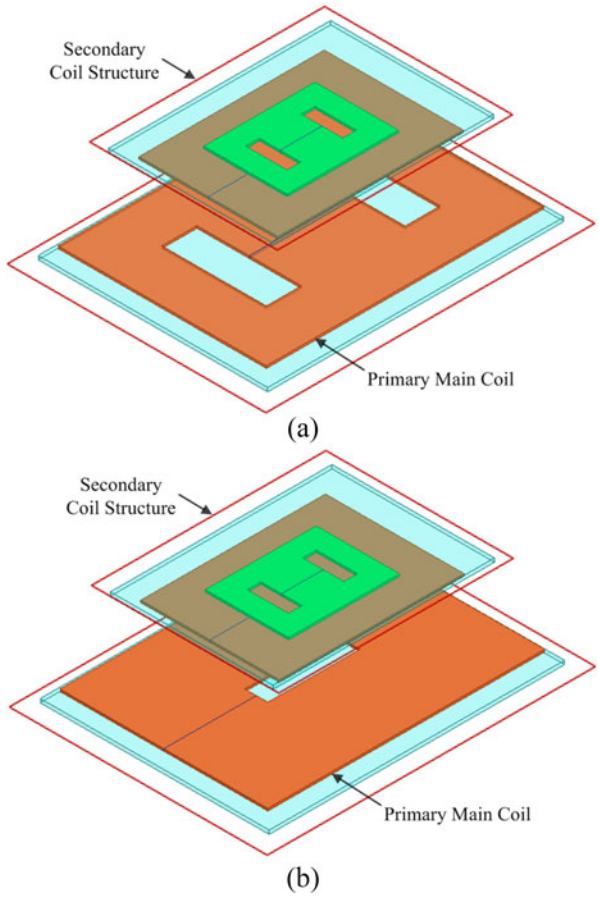

Fig. 14. Interoperability study with (a) primary bipolar coil and (b) primary unipolar coil.

TABLE VIII
INTEROPERABILITY STUDY

Primary main coil type	k		$k_1 f_2$	
	Simulation	Measured	Simulation	Measured
Bipolar	6.398×10^{-5}	7.241×10^{-5}	0.0564	0.0619
Unipolar	0.2310	0.2208	0.00014	0.0002

VI. CONCLUSION

In this paper, an integration method for unipolar coil structures in EV wireless charging systems using the *LCC* compensation topology is proposed. It effectively eliminates the extra coupling coefficients resulted from integration, simplifies the design, makes the system more compact, and keeps the outstanding system performance of a wireless charging system using the double-sided *LCC* compensation topology. The aspect ratios of compensated coils are analyzed to minimize the respective coupling coefficient through simulations. In addition, a wireless charging system with the proposed integration method is built and the experimental results demonstrate that the system is able to transfer 3.09 kW with a dc–dc efficiency of 95.49% at an air gap of 150 mm when fully aligned. Furthermore, a comparative study of the physical design parameters and system performance

between a wireless charging system with the proposed method and a wireless charging system with the integration into bipolar main coils has been conducted. The results show that the wireless charging system with the proposed integration is better because of its superior performance on EV's front-to-rear misalignment and vertical misalignment. Therefore, the proposed integration method is more applicable.

Our future work is to install the wireless charging system with the proposed integration method on a vehicle. Specifically, our work is focused on two aspects: 1) further optimize the integrated compensated coils in order to improve the electromagnetic interference performance; and 2) design a foreign object detection system by employing arrays of auxiliary coils and adjust the threshold values according to the magnetic field generated by main coils and compensated coils.

REFERENCES

[1] S. Li and C. C. Mi, "Wireless power transfer for electric vehicle applications," *IEEE J. Emerg. Sel. Topics Power Electron.*, vol. 3, no. 1, pp. 4–17, Mar. 2015.

[2] C. C. Mi, G. Buja, S. Y. Choi, and C. T. Rim, "Modern advances in wireless power transfer systems for roadway powered electric vehicles," *IEEE Trans. Ind. Electron.*, vol. 63, no. 10, pp. 6533–6545, Oct. 2016.

[3] G. A. Covic and J. T. Boys, "Modern trends in inductive power transfer for transportation applications," *IEEE J. Emerg. Sel. Topics Power Electron.*, vol. 1, no. 1, pp. 28–41, May 2013.

[4] Z. Bi *et al.*, "A review of wireless power transfer for electric vehicles: Prospects to enhance sustainable mobility," *Appl. Energy*, vol. 179, pp. 413–425, Oct. 2016.

[5] H. Takanashi, Y. Sato, Y. Kaneko, S. Abe, and T. Yasuda, "A large air gap 3 kW wireless power transfer system for electric vehicles," in *Proc. IEEE Energy Convers. Congr. Expo.*, 2012, pp. 269–274.

[6] M. Budhia, G. A. Covic, and J. T. Boys, "Design and optimization of circular magnetic structures for lumped inductive power transfer systems," *IEEE Trans. Power Electron.*, vol. 26, no. 11, pp. 3096–3018, Apr. 2011.

[7] M. Budhia, J. T. Boys, G. A. Covic, and C. Huang, "Development of a single-sided flux magnetic coupler for electric vehicle IPT charging systems," *IEEE Trans. Ind. Electron.*, vol. 60, no. 1, pp. 318–328, Sep. 2011.

[8] T. Nguyen, S. Li, W. Li, and C. C. Mi, "Feasibility study on bipolar pads for efficient wireless power chargers," in *Proc. IEEE Appl. Power Electron. Conf. Expo.*, 2014, pp. 1676–1682.

[9] S. Y. Choi, J. Huh, W. Y. Lee, J. G. Cho, and C. T. Rim, "Asymmetric coil sets for wireless stationary EV chargers with large lateral tolerance by dominant field analysis," *IEEE Trans. Power Electron.*, vol. 29, no. 12, pp. 6406–6419, Dec. 2014.

[10] C. Park, S. Lee, S. Y. Jeong, G.-H. Cho, and C. T. Rim, "Uniform power I-type inductive power transfer system with DQ-power supply rails for on-line electric vehicles," *IEEE Trans. Power Electron.*, vol. 30, no. 11, pp. 6446–6455, Nov. 2015.

[11] W. Zhang, J. C. White, and C. C. Mi, "Loosely coupled transformer structure and interoperability study for EV wireless charging systems," *IEEE Trans. Power Electron.*, vol. 30, no. 11, pp. 6356–6367, Nov. 2015.

[12] A. Khaligh and S. Dusmez, "Comprehensive topological analysis of conductive and inductive charging solutions for plug-in electric vehicles," *IEEE Trans. Veh. Technol.*, vol. 61, no. 11, pp. 3475–3489, Aug. 2012.

[13] Z. U. Zahid *et al.*, "Modeling and control of series–series compensated inductive power transfer system," *IEEE J. Emerg. Sel. Topics Power Electron.*, vol. 3, no. 1, pp. 111–123, Mar. 2015.

[14] W. Zhang and C. C. Mi, "Compensation topologies of high-power wireless power transfer systems," *IEEE Trans. Veh. Technol.*, vol. 65, no. 6, pp. 4768–4778, Jun. 2016.

[15] S. Li, W. Li, J. Deng, T. D. Nguyen, and C. C. Mi, "A double-sided LCC compensation network and its tuning method for wireless power transfer," *IEEE Trans. Veh. Technol.*, vol. 64, no. 6, pp. 2261–2273, Aug. 2014.

[16] W. Li, H. Zhao, S. Li, J. Deng, T. Kan, and C. C. Mi, "Integrated LCC compensation topology for wireless charger in electric and plug-in electric vehicles," *IEEE Trans. Ind. Electron.*, vol. 62, no. 7, pp. 4215–4225, Dec. 2014.

[17] T. Kan, T. D. Nguyen, J. C. White, R. K. Malhan, and C. Mi, "A new integration method for an electric vehicle wireless charging system using LCC compensation topology: Analysis and design," *IEEE Trans. Power Electron.*, vol. 32, no. 2, pp. 1638–1650, Feb. 2017.

[18] Y. Li, R. Mai, L. Lu, and Z. He, "Active and reactive currents decomposition based control of angle and magnitude of current for a parallel multi-inverter IPT system," *IEEE Trans. Power Electron.*, vol. 32, no. 7, pp. 1602–1614, Feb. 2017.

[19] X. Zhang, T. Kan, C. You, and C. Mi, "Modeling and analysis of ac output power factor for wireless chargers in electric vehicles," *IEEE Trans. Power Electron.*, vol. 32, no. 2, pp. 1481–1492, Feb. 2017.

[20] J. Y. Lee and B. M. Han, "A bidirectional wireless power transfer EV charger using self-resonant PWM," *IEEE Trans. Power Electron.*, vol. 30, no. 4, pp. 1784–1787, Apr. 2015.

[21] A. Pevere, R. Petrella, C. C. Mi, and S. Zhou, "Design of a high efficiency 22 kW wireless power transfer system for EVs fast contactless charging stations," in *Proc. IEEE Electr. Veh. Conf.*, 2014, pp. 1–7.

[22] G. C. Jang, S. Y. Jeong, H. G. Kwak, and C. T. Rim, "Metal object detection circuit with non-overlapped coils for wireless EV chargers," in *Proc. IEEE 2nd Annu. Southern Power Electron. Conf.*, 2016, pp. 1–6.

[23] S. Y. Jeong, H. G. Kwak, G. C. Jang, and C. T. Rim, "Living object detection system based on comb pattern capacitive sensor for wireless EV chargers," in *Proc. IEEE 2nd Annu. Southern Power Electron. Conf.*, 2016, pp. 1–6.

[24] S. Y. Jeong, H. G. Kwk, G. C. Jang, S. Y. Choi, and C. T. Rim, "Dual-purpose non-overlapping coil sets as metal object and vehicle position detections for wireless stationary EV chargers," *IEEE Trans. Power Electron.*, vol. PP, no. 99, pp. 1–11, Oct. 2017, doi: 10.1109/TPEL.2017.2765521.

[25] G. Ombach, "Design and safety considerations of interoperable wireless charging system for automotive," in *Proc. 9th Int. Conf. Ecol. Veh. Renew. Energies*, Mar. 2014, pp. 1–4.

[26] S. Choi, B. Gu, S. W. Lee, W. Y. Lee, J. Huh, and C. T. Rim, "Generalized active EMF cancel methods for wireless electric vehicles," *IEEE Trans. Power Electron.*, vol. 29, no. 11, pp. 5770–5783, Nov. 2014.

[27] W. Zhang, J. White, R. Malhan, and C. Mi, "Loosely coupled transformer coil design to minimize EMF radiation in concerned areas," *IEEE Trans. Veh. Technol.*, vol. 65, no. 6, pp. 4779–4789, Jun. 2016.

[28] Z. Bi, L. Song, R. D. Kleine, C. Mi, and G. Keoleian, "Plug-in vs. wireless charging: Life cycle energy and greenhouse gas emissions for an electric bus system," *Appl. Energy*, vol. 146, pp. 11–19, 2015.

[29] B. Hesterman, "Analysis and modeling of magnetic coupling," *Denver Chapter, IEEE Power Electron. Soc.*, Univ. Colorado, Boulder, CO, USA, 2007.

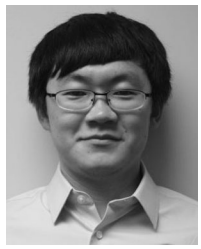

Tianze Kan (S'15) received the B.Eng. degree in electrical engineering and automation from the Huazhong University of Science and Technology, Wuhan, China, in 2011, and the M.S. degree in electrical engineering from the University of Southern California, Los Angeles, CA, USA, in 2013. He is currently working toward the Ph.D. degree in electrical and computer engineering in the joint doctoral program between San Diego State University, San Diego, CA, USA, and the University of California San Diego, La Jolla, CA, USA.

His research interests include power electronics and inductive-based wireless power transfer, especially on coil design and compensation topologies.

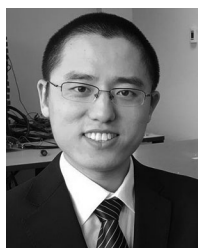

Fei Lu (S'12–M'17) received the B.S. and M.S. degrees from the Harbin Institute of Technology, Harbin, China, and the Ph.D. degree from the University of Michigan, Ann Arbor, MI, USA, in 2010, 2012, and 2017, respectively, all in electrical engineering.

He is working on the high-power and high-efficiency capacitive power transfer through an air-gap distance up to 100s of millimeters. He is also working on the application of wide band-gap devices on the wireless power transfer system to increase the system frequency. His research interest focuses on wireless power transfer for the application of electric vehicle charging.

Trong-Duy Nguyen was born in Binh Dinh, Vietnam. He received the B.Eng. and M.Eng. degrees from the Ho Chi Minh City University of Technology, Ho Chi Minh City, Vietnam, in 2004 and 2007, respectively, and the Ph.D. degree from the Nanyang Technological University, Singapore, in 2012, all in electrical and electronic engineering.

His current research interests include vehicle control system development, electromagnetics, and electrical machine drives.

Patrick P. Mercier (S'04–M'12–SM'17) received the B.Sc. degree in electrical and computer engineering from the University of Alberta, Edmonton, AB, Canada, in 2006, and the S.M. and Ph.D. degrees in electrical engineering and computer science from the Massachusetts Institute of Technology (MIT), Cambridge, MA, USA, in 2008 and 2012, respectively.

He is currently an Assistant Professor in electrical and computer engineering with the University of California San Diego (UCSD), La Jolla, CA, USA, where he is also the co-Director of the Center for Wearable Sensors. He was the Co-Editor of *Ultra-Low-Power Short Range Radios* (Springer, 2015) and *Power Management Integrated Circuits* (CRC Press, 2016). His research interests include the design of energy-efficient microsystems, focusing on the design of RF circuits, power converters, and sensor interfaces for miniaturized systems and biomedical applications.

Prof. Mercier has served as an Associate Editor for the IEEE TRANSACTIONS ON VERY LARGE SCALE INTEGRATION from 2015 to 2017. Since 2013, he has been serving as an Associated Editor for the IEEE TRANSACTIONS ON BIOMEDICAL INTEGRATED CIRCUITS, and since 2017, has been a Member of the IEEE International Solid-State Circuits Conference (ISSCC) International Technical Program Committee (Technology Directions Sub-Committee) and CICC Technical Program Committee. He was the recipient of a Natural Sciences and Engineering Council of Canada (NSERC) Julie Payette fellowship in 2006, NSERC Postgraduate Scholarships in 2007 and 2009, an Intel Ph.D. Fellowship in 2009, the 2009 ISSCC Jack Kilby Award for Outstanding Student Paper at ISSCC 2010, a Graduate Teaching Award in Electrical and Computer Engineering at UCSD in 2013, the Hellman Fellowship Award in 2014, the Beckman Young Investigator Award in 2015, the DARPA Young Faculty Award in 2015, the UC San Diego Academic Senate Distinguished Teaching Award in 2016, and the Biocom Catalyst Award in 2017.

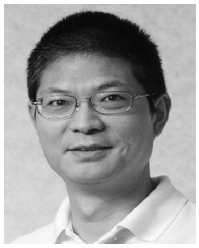

Chunting Chris Mi (S'00–A'01–M'01–SM'03–F'12) received the B.S.E.E. and M.S.E.E. degrees from Northwestern Polytechnical University, Xi'an, China, in 1985 and 1988, respectively, and the Ph.D. degree from the University of Toronto, Toronto, ON, Canada, in 2001, all in electrical engineering.

He is a Professor and the Chair of electrical and computer engineering and the Director of the Department of Energy funded Graduate Automotive Technology Education Center for Electric Drive Transportation, San Diego State University (SDSU), San Diego, CA, USA. Prior to joining SDSU, he was with University of Michigan, Dearborn, from 2001 to 2015. He was the President and the Chief Technical Officer of 1Power Solutions, Inc., from 2008 to 2011. He is the Co-Founder of Gannon Motors and Controls LLC and Mia Motors, Inc. He has conducted extensive research and has authored or co-authored more than 100 journal papers. He has taught tutorials and seminars on the subject of hybrid electric vehicles/plug-in hybrid electric vehicles for the Society of Automotive Engineers (SAE), the IEEE, workshops sponsored by the National Science Foundation, and the National Society of Professional Engineers. He has delivered courses to major automotive OEMs and suppliers, including GM, Ford, Chrysler, Honda, Hyundai, Tyco Electronics, A&D Technology, Johnson Controls, Quantum Technology, Delphi, and the European Ph.D. School. He has offered tutorials in many countries, including the U.S., China, South Korea, Singapore, Italy, France, and Mexico. He has authored or co-authored more than 100 articles and delivered 30 invited talks and keynote speeches. His research interests include electric drives, power electronics, electric machines, renewable-energy systems, and electrical and hybrid vehicles.

Dr. Mi is the recipient of "Distinguished Teaching Award" and "Distinguished Research Award" of the University of Michigan-Dearborn, the 2007 IEEE Region 4 "Outstanding Engineer Award," "IEEE Southeastern Michigan Section Outstanding Professional Award," and the "SAE Environmental Excellence in Transportation (E2T)." He has also served as a panelist in major IEEE and SAE conferences.